JOURNAL OF GEOPHYSICAL RESEARCH, VOL. 104, NO. A12, PAGES 28,073–28,088, DECEMBER 1, 1999

Consequences of geomagnetic history on the high-latitude thermosphere and ionosphere: Averages

Anasuya L. Aruliah and Ingo C.F. Müller-Wodarg,

Atmospheric Physics Laboratory, University College London, London

Jacqueline Schoendorf [1]

Department of Electrical and Computer Engineering and Center for Space Physics, Boston University Boston, Massachusetts

Abstract. The thermospheric effects of "geomagnetic history" and the resulting ion-neutral interactions are determined through the analysis of a long-term database of high latitude neutral winds from Kiruna, Sweden, and simulations with the coupled thermosphere ionosphere plasmasphere model (CTIP). Three types of geomagnetic history are examined in detail with the data and the model: steady state conditions in which the *Kp* index for the current three hours is the same as the *Kp* index for the previous 3 hours; previously quiet conditions in which the *Kp* index for the current 3 hours is greater than the *Kp* index for the previous 3 hours; and previously active conditions in which the *Kp* index for the current 3 hours is less than the *Kp* index for the previous 3 hours. It is shown that during the hours of darkness at Kiruna, while the ionosphere responds immediately to changes in activity, the neutral gas can take between 3 and 6 hours to recover from the effects of any previous activity. Model simulations show that the rate of energy dissipation is also significantly dependent on geomagnetic history. For the previously active case the Joule heating and mechanical energy transfer rate are up to 4 times larger at certain latitudes as the steady state case. For the previously quiet case the heating rates are much smaller than the steady state case. There is a frequently made assumption that at high latitudes the mechanical energy transfer rate may be ignored as insignificant compared with the Joule heating rate. The results presented here show that this assumption is unreliable, particularly in the dusk sector and polar cap.

1. Introduction

It is well acknowledged that the neutral gas has a large inertia compared with the plasma constituent of the upper atmosphere since it is 99.9% of the mass. The rule of thumb is that the response time of thermospheric winds to changes in the plasma motion may be calculated using the inverse of the neutral-ion collision frequency, ν_{ni} [e.g., *Rishbeth and Garriott*, 1969]. During the nighttime hours, this is approximately 1-2 hours, which corresponds to electron densities of around $5x10^{11}m^{-3}$ in the *F*-region. However, the consequences of this delay do not appear to have been investigated systematically. In particular, with empirical studies of the ionosphere there is a commonly made assumption that the average neutral wind is zero, or some constant value [e.g., *Brekke*, 1976, *Foster et al.*, 1983]. As a result, there is little acknowledgment of the effect of "geomagnetic history" in studies of the upper atmosphere. (In this paper geomagnetic history is defined by considering the *Kp* value for the previous 3 hour interval to that when a measurement was made.) Yet storm studies, which are particularly important for magnetosphere-ionosphere coupling studies, are dealing with highly variable geomagnetic activity conditions when neglecting the neutral wind response will distort any calculation of the energy budget. This paper will present both empirical and model data demonstrating the consequences of two examples of geomagnetic history: previously active and previously quiet conditions. Comparisons are made with steady state models to illustrate that there are significant differences caused purely by the inertia of the neutral winds. Without acknowledgment of the importance of this effect it is likely that these differences may be wrongly interpreted.

2. Analysis of Long-Term Average Winds

Upper thermospheric wind measurements were analyzed for the effects of geomagnetic history. The winds were measured using a Fabry-Perot interferometer (FPI) at Kiruna, Sweden (67.8°N, 20.4°E), which is an auroral site (details given by *Aruliah et al.* [1996]). The FPI measures the O I emission at a wavelength of 630 nm. This emission peaks at a height of around 240 km. The database extends back to the winter of

[1] Now at Mission Research Corporation, Nashua, New Hampshire.

Copyright 1999 by the American Geophysical Union.

Paper number 1999JA900334.
0148-0227/99/1999JA900334$09.00

1981-1982 and is divided approximately in two to represent solar maximum and solar minimum. Average winds are calculated from six solar maximum winters (generally between September and April, inclusive) which span the years of 1981-1982, 1982-1983, 1988-1989, 1989-1990, 1990-1991 and 1991-1992. The average value of the solar flux index for all these data is $F_{10.7}$ = 185 ±20. Ionospheric data from the EISCAT radar for the same period were also analyzed, but there was no indication of geomagnetic history effects in the average ion velocities and therefore data are not shown here. This reinforces the results of previous investigators who have shown that the response of plasma flows to changes in the high-latitude electric field is almost immediate [e.g., *Etemadi et al.*, 1988].

The data are sorted into three geomagnetic activity levels, quiet (q), moderate (m) and active (a), using the *Kp* index in the following manner:

$0 \le Kp < 2$	quiet (q),
$2 \le Kp < 4$	moderately active (m),
$4 \le Kp < 6$	active (a)

The *Kp* index gives the geomagnetic activity for every 3 hour period during a day, beginning with 0000-0300 UT. Then, in order to account for geomagnetic history, the data are sorted using three criteria: (1) steady state (ss), i.e., each data point is chosen so that the previous 3 hour *Kp* index is in the same *Kp* range; (2) previously active (pa), that is, the previous 3 hour *Kp* index is in the higher *Kp* range, and (3) previously quiet (pq), that is, the previous 3 hour *Kp* index is in the lower *Kp* range. Table 1 indicates the number of data points in each 15 min interval, and also the abbreviations used in the paper for each data subset, for example, pq(q) for geomagnetically quiet data that are also previously quiet.

Figure 1 illustrates the trends in the steady state average meridional and zonal thermospheric winds for each of the three levels of geomagnetic activity at solar maximum. It is clearly apparent that there is a strong dependence on geomagnetic activity. The top plot (Figure 1a) shows the variation through the night (UT denotes universal time) of the meridional component (+ve southward) observed to the north of Kiruna and the bottom (Figure 1b) shows the zonal component (+ve eastward) observed to the west. Data are averaged at 15 min intervals. The vertical bars show the standard error of the mean. There are 42 ± 15 nights contributing to the average meridional winds for geomagnetically quiet conditions, 77 ± 35 for moderate activity, and 30 ±14 for active conditions. Owing to the large seasonal variation in the length of the night at high latitudes, the smallest sample size for any 15 min interval is at the beginning and end of the night. The data contributing to these periods of time will be from the longest nights in the middle of winter when the observing period is 17-18 hours long. The main trends to look out for are as follows:

1) During the period 1500-1800 UT the zonal winds are very sensitive to the level of geomagnetic activity. For $0 \le Kp < 2$, Kiruna is on the outer edge of the auroral oval. Consequently, the pressure gradient is the dominant force on the neutral gas, and thus the flow is mainly eastward. With increasing geomagnetic activity, the auroral oval expands in size so that for moderately active conditions Kiruna is within the auroral oval during the night. Under these conditions the ion drag force is larger, and the neutrals become drawn into the ion convection pattern. Thus the zonal winds in this time period become increasingly westward flowing as *Kp* increases. However, the meridional winds show little dependence on *Kp*.

2) The period 1800-2400 UT includes observation of the Harang discontinuity, when the plasma flow swaps from a westward to an eastward flow. It delineates the dusk and dawn auroral ovals. The magnitude and direction of the winds in this period are a sensitive indicator of the level of geomagnetic activity. There is a small trend in the zonal winds so that the time of the changeover for the neutral gas becomes earlier with increasing activity. This agrees with the general trend with respect to geomagnetic activity shown in average electric field models such as *Foster et al.* [1986]. Thus at the latitude of Kiruna (65° magnetic latitude, MLT = UT+3 hours) the two-cell configuration expands equatorward and twists around with increasing activity so that the Harang discontinuity occurs at earlier MLT values. The major difference, though, is seen in the average meridional winds when the winds in the most active range of *Kp* ($4 \le Kp < 6$) are more than double the size of those in the quietest range ($0 \le Kp < 2$). Also the zonal winds before 2100 UT are small and eastward for $0 \le Kp < 2$, but large and westward for the more active ranges. As with the period1500-1800 UT, these changes represent the increase in size of the auroral oval with *Kp* and the increase in ion drag on the neutral gas.

3) During the period 0300-0600 UT there is a large difference in the times when the zonal winds change from an eastward to westward flow. The average zonal winds in the quietest range ($0 \le Kp < 2$) change direction 2 hours earlier than those in the most active range of *Kp* ($4 \le Kp < 6$). This is related to the size of the auroral oval. The eastward flow is driven by the sunward ionospheric convection, while the westward flow is seen when Kiruna has passed outside of the auroral oval; which is when the antisunward pressure gradients dominate the neutral flow. Thus at higher activity levels, when the auroral oval is expanded, Kiruna sees eastward flow for a longer time.

It is important to note that the average winds shown in the figures are statistical constructs. The data are binned according to the 3 hour interval they fall into, beginning with 0000-0300 UT. For example, all data collected in the interval 1800-2100

Table 1. Types of Geomagnetic History Classifications

Classification	Current 3 hours have *Kp* of: Quiet (q) $0 \le Kp < 2$	Moderate (m) $2 \le Kp < 4$	Active (a) $4 \le Kp < 6$
Previously Quiet (pq)	pq(q)	pq(m)	pq(a)
Kp range for previous 3 hours	X	$Kp \le 2$	$Kp \le 4$
$< N >$	X	20 ± 8	18 ± 8
Steady State (ss)	ss(q)	ss(m)	ss(a)
Kp range for previous 3 hours	$0 \le Kp < 2$	$2 \le Kp < 4$	$4 \le Kp < 6$
$< N >$	42 ± 15	77 ± 35	30±14
Previously Active (pa)	pa(q)	pa(m)	pa(a)
Kp range for previous 3 hours	$Kp \ge 2$	$Kp \ge 4$	X
$< N >$	16 ±10	17 ±8	X

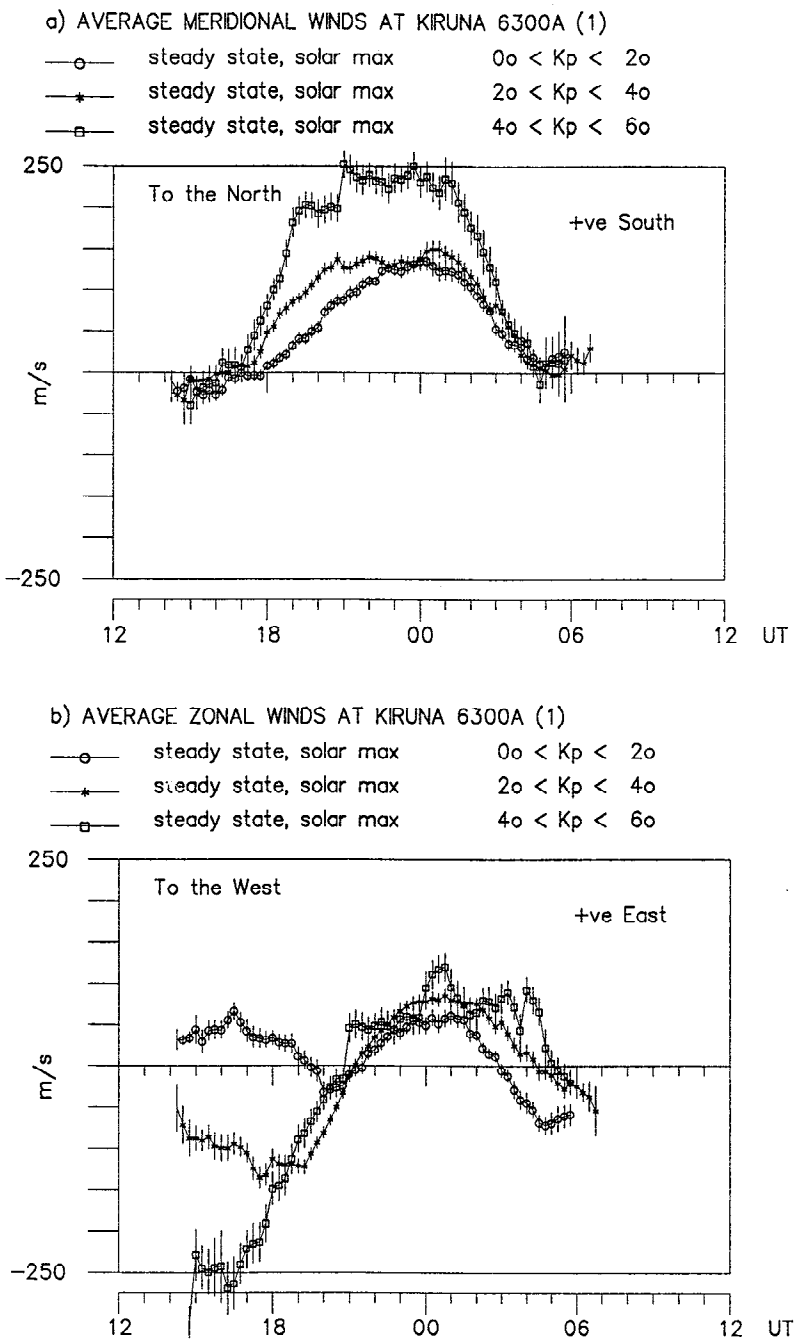

Figure 1. Trends in the steady state average meridional and zonal thermospheric winds as geomagnetic activity increases. Three levels of geomagnetic activity are plotted: $0 \leq Kp < 2$ (quiet), $2 \leq Kp < 4$ (moderately active), $4 \leq Kp < 6$ (active) showing the variation through the night (UT is universal time; Kiruna local time is UT+1 hour) of (a) the meridional component (+ve southward) observed to the north of Kiruna and (b) the zonal component (+ve eastward) observed to the west.

UT are binned according to the *Kp* for that interval. However, the *Kp* for the previous 3 hour interval, in this case 1500-1800UT, decides whether the classification is previously quiet (pq), steady state (ss), or previously active (pa). This form of binning means that each 3 hour interval should be judged separately. The figures do not show the behavior throughout a night of the average wind for a given subset because the average wind for each 3 hour interval is unrelated to the average wind for the previous or following 3 hour interval by definition. For example, the average winds for 1800-2100 UT of the subset pq(m) (i.e. previously quiet, moderate activity) are calculated from all data collected between 1800 and 2100 UT for which $2 \leq Kp < 4$, and $Kp \leq 2$ for the previous 3 hours (1500-1800 UT). This means that all nights qualifying for this subset, pq(m), must have the period 1800-2100 UT classified as moderate and 1500-1800 UT classified as quiet. As a result, each 3 hour period of the pa or pq data sets will be the average of different nights from the previous 3 hour period. The

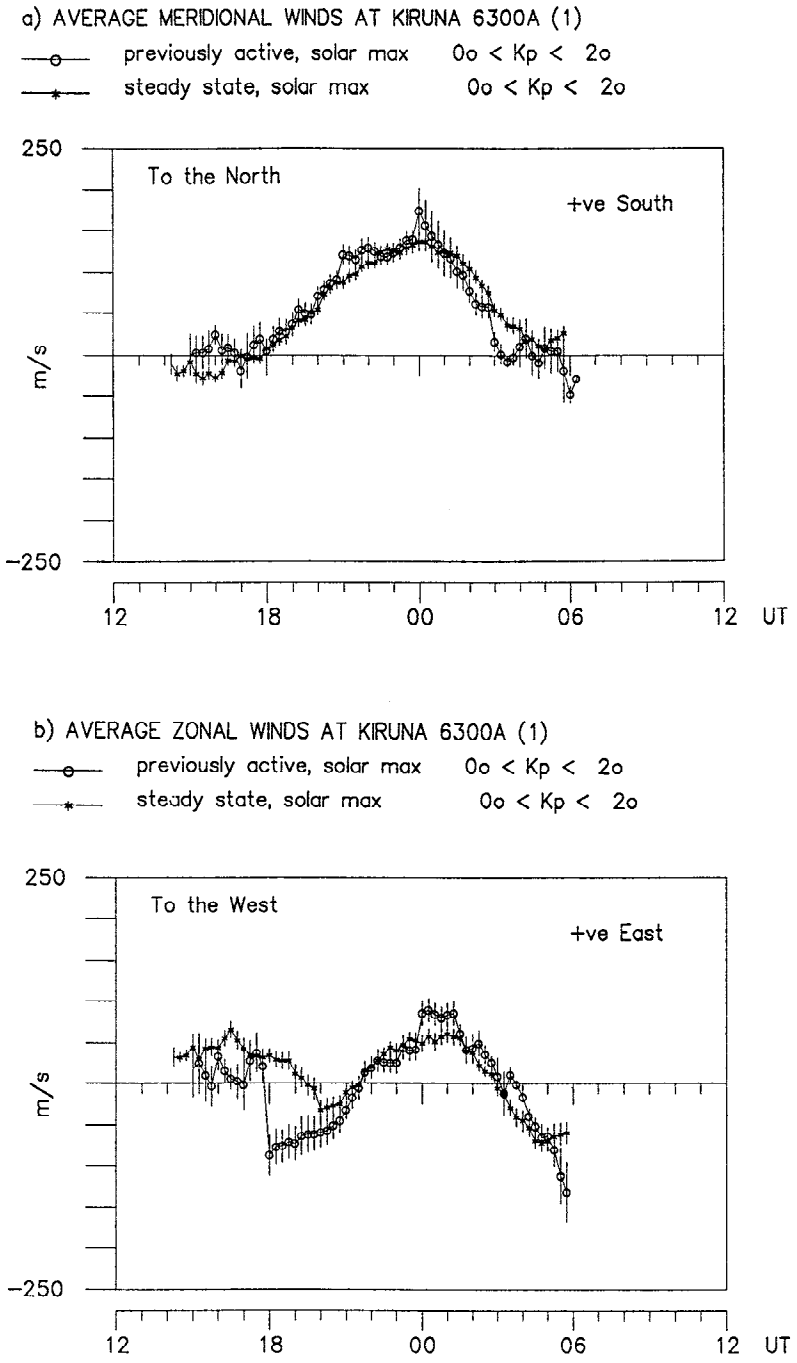

Figure 2. Fabry-Perot interferometer (FPI) average winds for solar maximum, geomagnetically quiet ($0 \leq Kp < 2$) conditions, comparing steady state and previously active average winds. Each 3 hour interval must be judged separately (see text for explanation). Although the winds from individual nights have been selected so that the *Kp* value current with the measurement is in the same range ($0 \leq Kp < 2$), the average winds for the pa(q) case are typical of more active conditions than the ss(q) case.

discontinuities seen in the pq and pa average winds between the end of one 3 hour period and the beginning of the next reveal this.

The steady state data sets show a smoother variation between each 3 hour period because the definition of steady state allows data from the same nights for consecutive 3 hour periods. The sample sizes of these data sets are larger, which implies that the steady state is more common than large, rapid variations in geomagnetic activity.

Figure 2 shows FPI average winds for solar maximum, geomagnetically quiet (q) ($0 \leq Kp < 2$) conditions, comparing steady state and previously active average winds. There is a small, but statistically significant difference between the two sets of winds. The implication is that the pa(q) average winds are recovering from the past higher levels of activity, and therefore the overall wind magnitude is larger and the zonal winds in the period 1500-2000UT are less eastward/more westward than the ss(q) average winds.

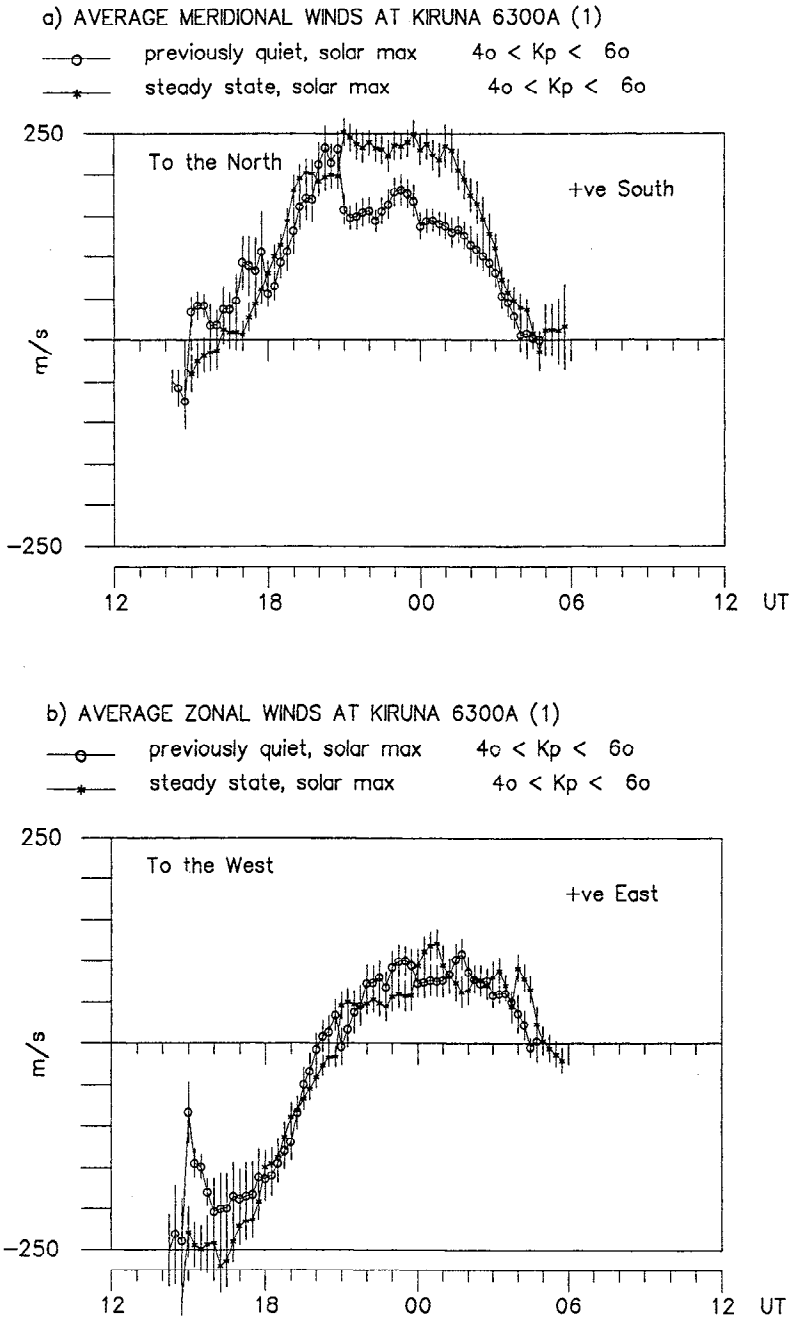

Figure 3. FPI average winds for solar maximum, geomagnetically active ($4 \leq Kp < 6$) conditions, comparing steady state and previously quiet average winds. Each 3 hour interval must be judged separately (see text for explanation). Although the winds from individual nights have been selected so that the *Kp* value current with the measurement is in the same range ($4 \leq Kp < 6$), the average winds for the pq(a) case are typical of quieter conditions than the ss(a) case.

Figure 3 shows FPI average winds for solar maximum, geomagnetically active (a) ($4 \leq Kp < 6$) conditions, comparing steady state and previously quiet average winds. There is a considerable and statistically significant difference between the two sets of winds. The implication is that the pq(a) average winds still retain the memory of the previously quiet conditions owing to inertia, and therefore the overall wind magnitude is smaller and the zonal winds in the period 1500-2000 UT are less westward than the ss(a) average winds. In other words, the pq(a) winds are more typical of a lower *Kp* range.

On inspecting Figures 2 and 3 it is noticeable that the difference between the ss(q) and pa(q) meridional winds in Figure 2 is very small, while there is a large difference between the ss(a) and pq(a) meridional winds in Figure 3. This can be related back to the trend with geomagnetic activity shown in Figure 1. The difference between the meridional winds for the quiet and moderately active states is less than that between moderately active and active states. In other words, the trend is not linear. In contrast, the trend in the zonal winds is roughly linear.

Another interesting point is that the difference between the ss(a) and pq(a) meridional winds in Figure 3 before 2100 UT is small, and large after this time. It may be possible that there is a residual effect from the large electron densities on the dayside, which increases the ion-neutral coupling and therefore shortens the time taken for the neutrals to revert to the steady state condition.

3. Modeling Results

The effects and consequences of geomagnetic history at high latitudes were modeled using the coupled thermosphere ionosphere plasmasphere model (CTIP) [*Fuller-Rowell et al.*, 1996, *Millward et al.*, 1996, and references therein].The model simulations enable a qualitative analysis of the effects of geomagnetic history. A rough quantitative analysis is also possible, which may then be used as a guide for future interpretations of the behavior of the upper atmosphere.

The CTIP model solves self-consistently the three-dimensional coupled nonlinear equations of momentum, energy, and continuity for neutral species (O, O_2, N_2) and ions (O+, H+) above 80 km altitude. This model, and earlier versions, have been used extensively in upper atmosphere studies since the early 1980s, most recently to investigate the response to geomagnetic storms [e.g., *Field et al.*, 1998], as well as thermospheric circulation and composition [*Müller-Wodarg and Aylward*, 1998; *Rishbeth and Müller-Wodarg*, 1999].

Thermospheric calculations are carried out on an Eulerian frame of reference that is a spherical corotating grid with a resolution of 2° in latitude and 18° in longitude. Vertically, the neutral atmosphere above 80 km is divided into 15 levels of constant pressure, spaced at one scale height, reaching an altitude of around 400 km (depending on solar and magnetic activity). Ionospheric calculations are carried out on a Lagrangian frame which has been modified to be compatible with the Eulerian frame by being referenced to a fixed Sun-Earth axis [*Fuller-Rowell et al.*, 1987]. It uses the same horizontal spacing as the thermospheric frame, but in the vertical direction there are 86 levels of constant height between 100 km and around 10,000 km altitude. The time step for calculations is 60 s. The CTIP model uses a geomagnetic field with offset poles, situated at 81°N/78°W and 74°S/126°E, which are surrounded by the auroral oval belts. The high-latitude electric field is given by the statistical model of *Foster et al.* [1986], and the auroral particle precipitation is taken from the statistical model of *Fuller-Rowell and Evans* [1987].

All simulations were carried out for December solstice, with an $F_{10.7}$ solar flux index of 200. This value of solar flux is within a standard deviation of the average value of solar flux experienced by the FPI average winds. As can be seen in Figure 1, and explained earlier, the most clearly defined differences between the different geomagnetic activity levels are apparent mainly in the zonal winds within the three intervals: 1500-1800 UT, 1800-2100 UT and 0300-0600 UT. These periods have been identified as most useful for investigating the balance between the two dominant driving forces at high latitudes, that is, the pressure gradient and ion drag. For each of these three intervals the geomagnetic activity was reduced/increased by altering appropriately the high-latitude electric field for the previous 6 hours to represent previously quiet/active conditions. The high-latitude energy source from magnetospheric particle precipitation was also varied to complement the changes in the electric field. Measurements from the NOAA/TIROS satellites have been parameterized by *Fuller-Rowell and Evans* [1987], and from these, TIROS levels 3 (Kp =1+, cross polar cap potential difference (CPCPD)=26 kV), 6 (Kp =3-, CPCPD=46 kV) and 9 (Kp =5-, CPCPD=79 kV) were chosen to define the three activity levels so that they roughly correspond with the levels used to bin the FPI winds. Although the simulations are meant for comparison with Figures 2 and 3, where only the previous 3 hours are taken into account, the following results show that it takes around 6 hours for the influence of the previous level of activity to be removed. This is the reason for maintaining the lower/higher electric field and particle precipitation for a 6 hour period in these simulations, so as to have a distinct signature of the higher or lower activity levels when looking for geomagnetic history effects. Only the results for the period 1800-2100 UT are shown here, since the other periods lead to similar conclusions.

Figure 4 shows the CTIP simulation on the model grid point closest to Kiruna, at pressure level 12, which is a pressure of 1.7×10^{-5} Pa, and equivalent to a height of about 240 km, which is an appropriate height to be compared with the average winds shown in Figure 2. The simulation is for solar maximum ($F_{10.7}$ =200), geomagnetically quiet conditions ($0 \le Kp < 2$) comparing steady state and previously active average winds. The steady state situation is modeled using Tiros level 3 for the whole 24 hour period. For the previously active simulation the model uses TIROS level 3 for 18 hours, but sets the TIROS level to 6 for nearly 6 hours before 1800 UT, that is, between 1212 UT and 1748 UT, inclusive. The comparison between Figures 2 and 4 is for the 3 hour interval 1800-2100 UT only. However, the interval 1800-0000 UT is plotted to show how all the parameters of the pa(q) simulation revert close to the ss(q) condition in around 6 hours. It is worth mentioning again that the FPI average winds for the period 2100-0000 UT are not for comparison with the model results shown here because those average winds were compiled by assuming that the period 1800-2100 UT was more active, that is, $Kp \ge 2$.

Four parameters are plotted in Figure 4. These are southward wind component (Figure 4a), eastward wind component (Figure 4b), southward ion drag (Figure 4c), and eastward ion drag (Figure 4d). The final plot, Figure 4e, shows how the TIROS level was varied over the 24 hour simulation.The trends in the modeled zonal (Figure 4b) wind component generally follow well those seen in the FPI average winds in Figure 2b.The pa(q) zonal wind is strongly westward, while the ss(q) zonal wind is eastward. However, the modeled meridional wind components do not match the FPI average winds plotted in Figure 2a. The pa(q) neutral winds are less southward than the ss(q) because a large part of the momentum is being diverted into the zonal component. This shows that the ss(q) winds are dominated by the pressure gradients that drive the winds in an antisunward direction, which means eastward in the evening sector and southward in the midnight sector. This is expected because Kiruna is just outside the auroral oval when Kp=1+. In contrast, the pa(q) winds strongly follow the westward direction of the ion convection pattern, which is typical of an extended auroral oval, despite the fact that the electric field and particle precipitation patterns over this whole period are for Kp= 1+. The simulated winds for the pa(q) case show much greater ion-neutral coupling than the FPI average winds, because the simulated winds are more entrained in the plasma flow, and consequently have a larger westward than southward component. The difference between the simulation and the FPI average winds is due to the choice of electric field and particle

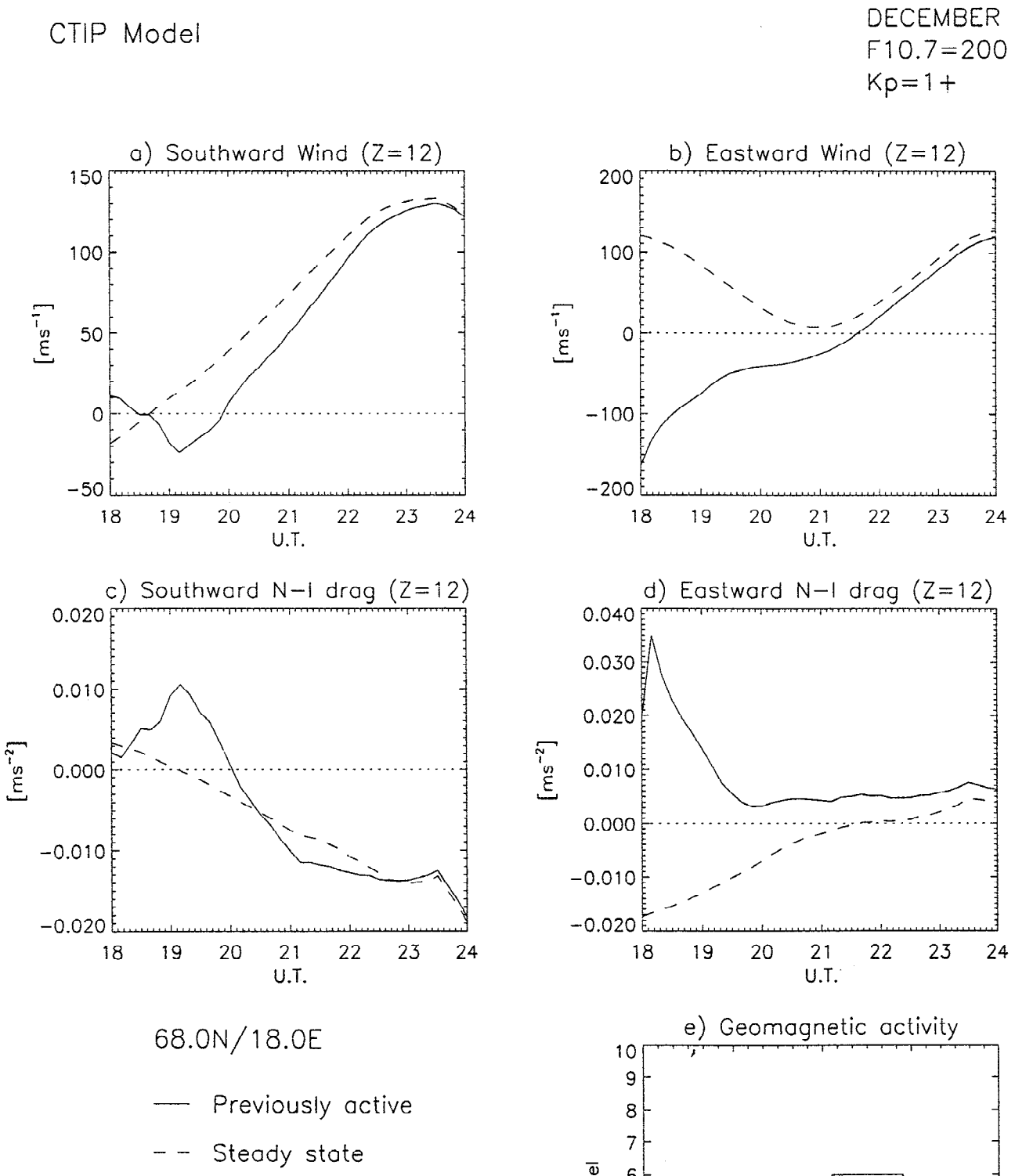

Figure 4. Local values from a coupled thermosphere ionosphere plasmasphere (CTIP) model simulation at Kiruna, pressure level 12 (around 240 km) for 1800-2400 UT, solar maximum, geomagnetically quiet conditions ($0 \leq Kp < 2$) comparing steady state and previously active average winds. The data shown are (a) southward wind component, (b) eastward wind component, (c) southward ion drag, (d) eastward ion drag, and (e) variation with time of the geomagnetic activity level. The trends in the modeled meridional and zonal wind components follow those seen in the FPI average winds in Figure 2 over the same period.

precipitation model. The agreement between the meridional winds could be improved by fine-tuning the choice of the electric field and precipitation models, but the point has been made, which is that the driving forces of the previous 6 hours are seen to persist for several hours after they have been tuned down.

There is a large spike in the eastward component of the ion drag (Figure 4d). This appears to a lesser extent in the southward component (Figure 4c), which is an order of magnitude smaller. This is evidence of the significant difference in the response of the neutrals and the ions. The neutral winds shown in Figures 4a and 4b change slowly and smoothly, despite the large jump in the forcing term from $Kp = 3-$ to $Kp = 1+$. However, the ions respond almost immediately, resulting in a rapid increase in the value of $(\mathbf{V}_i - \mathbf{U}_n)$, which is part of the ion drag term (here $\mathbf{V}_i$ is the ion velocity, $\mathbf{U}_n$ is the neutral velocity and the ion drag is $\nu_{ni}(\mathbf{V}_i - \mathbf{U}_n)$). It is also apparent that the components of the ion drag force are significantly southward and eastward, respectively, for the pa(q) winds. What this means is that the neutral winds are now moving faster than the ions owing to the residual momentum built up during the previous 6 hours. In the *E*- region this means that the neutral gas is continuing to drive a current despite the electric field and particle precipitation being dropped to a lower level. It is therefore an example of the neutral winds having a dynamo action, that is, storing up mechanical energy and subsequently releasing it as electrical energy. Such behavior has been predicted previously by *Lyons et al.* [1985] and *Deng et al.* [1993], who simulated the neutral dynamo effect (also called the flywheel effect) after a geomagnetic storm by suddenly turning off strong magnetospheric forcing and watching the atmosphere wind down afterward. There are plans with the assimilated mapping of ionospheric electrodynamics (AMIE) model to introduce feedback from the electric field generated by the neutral wind dynamo to modify the electric field generated by the magnetospheric dynamo [*Lu et al.*, 1995], but, although developed, it has not yet been implemented in the "standard" CTIP model. Eventually, the previously active neutral atmosphere is slowed down back to the steady state condition. Consequently, all the parameters for the previously active condition shown in Figures 4a-4d return back to the steady state values by the time 6 hours have passed.

The importance of the comparison shown in Figure 4 is that although the magnetospheric dynamo is supposed to be overwhelmingly dominant in the polar regions, here is an example of a common situation when the neutral wind dynamo cannot be ignored, that is, a previously active state. Any study of a non-steady-state situation, such as the recovery stage after a storm, should consider the potential contribution of the neutral wind dynamo. *Gary et al.* [1994] showed that the DE- 2 satellite measured a net upward Poynting flux for a considerable distance along the satellite track during a period of B_z north (=1.4 nT). This means a net upward flux of energy from the ionosphere to the magnetosphere. They attribute this to the weak solar wind-magnetospheric coupling with this IMF orientation, which means that there was no well-defined ion convection pattern. As a result, the neutral wind velocity was able to exceed the ion velocity. A previously active situation will be similar because the neutral gas will have been wound up by the previous geomagnetic activity and then will take some time to wind down. Meanwhile, the ionosphere will have responded almost immediately to the changes in the solar wind-magnetospheric coupling; thus the situation is created where the neutral gas is moving faster than the ions.

Figure 5 shows the CTIP simulation for 1800-2400 UT, solar maximum, geomagnetically active conditions ($4 \le Kp < 6$) comparing steady state and previously quiet average winds. The steady state situation is modeled using TIROS level 9 for the whole 24 hour period. For the previously quiet simulation the model uses TIROS level 9 for 18 hours, but sets the TIROS level to 6 for nearly six hours before 1800 UT, that is, between 1212 UT and 1748 UT, inclusive (see Figure 5e). Although the model wind magnitudes are much larger, the trends in the modeled meridional and zonal wind components follow those seen in the FPI average winds in Figure 3. Thus the pq(a) meridional winds (Figure 5a) are less southward and the zonal winds (Figure 5b) less westward than the ss(a) winds. In the evening sector the plasma flow is strongly westward for active conditions, while the pressure gradient drives the winds eastward. The pq(a) winds therefore typify more quiet conditions than the ss(a) winds. This means that a comparison of ion drag shown in Figures 5c and 5d shows that after 1800 UT, when the activity level is returned to TIROS level 9, the plasma is accelerating the neutrals more strongly for the pq(a) case, thus bringing the neutrals up to speed to match the ss(a) condition. As with the pa(q) case shown in Figures 4c and 4d, there is an initial sharp spike in the pq(a) ion drag data because the ion velocities respond almost immediately to the change in the geomagnetic forcing, while the neutrals respond more slowly and smoothly. After about 6 hours all the parameters for the pq(a) case, except the meridional winds, have returned close to the ss(a) values. This is about the same time as the pa(q) case takes to return to the ss(q) condition.

4. Joule Heating Versus Mechanical Energy Transfer Rates

A key to understanding the importance of geomagnetic history is to look at the energy transfer in the ionosphere. Energy is dissipated in the ionosphere as Joule heating, but there is also a conversion of energy from mechanical to electrical or vice versa which is brought about through the neutral winds. This has been discussed in some detail by, in particular, *Thayer et al.* [1995] and *Lu et al.* [1995], who have modeled steady state situations and theoretically separated the Joule heating from the mechanical energy transfer rate. They have used the argument of *Kelley et al.* [1991] with respect to simplifying the calculation of the total electromagnetic energy flux into the ionosphere (i.e., the Poynting flux), which is equal to the power dissipated in the ionosphere. In the steady state the Poynting flux is equal to the height-integrated energy transfer rate, $\mathbf{J}.\mathbf{E}$ [*Thayer et al.*, 1995].

$$\int \mathbf{J}.\mathbf{E}\, dz = \int \mathbf{J}.(\mathbf{E}' - \mathbf{U}_n \hat{} \mathbf{B})\, dz. \qquad (1)$$

= Joule heating + mechanical energy transfer rate.

Equation (1) explicitly shows the neutral wind contribution to the height-integrated energy transfer rate since the measured electric field, $\mathbf{E}$, is in the Earth frame and is related to the field in the wind frame, $\mathbf{E}'$, by the expression $\mathbf{E}' = \mathbf{E} + \mathbf{U}_n \hat{} \mathbf{B}$; where $(\mathbf{U}_n \hat{} \mathbf{B})$ is the electric field induced by the neutral wind which is moving with velocity $\mathbf{U}_n$ by driving ions across magnetic field lines, $\mathbf{B}$ (also called Lorentz forcing) [e.g., *Rishbeth*, 1997].

An analysis of the $\mathbf{J}.\mathbf{E}$ integral breaks down into two terms with the first being the Joule heating rate, $\mathbf{J}.\mathbf{E}'$. This is the

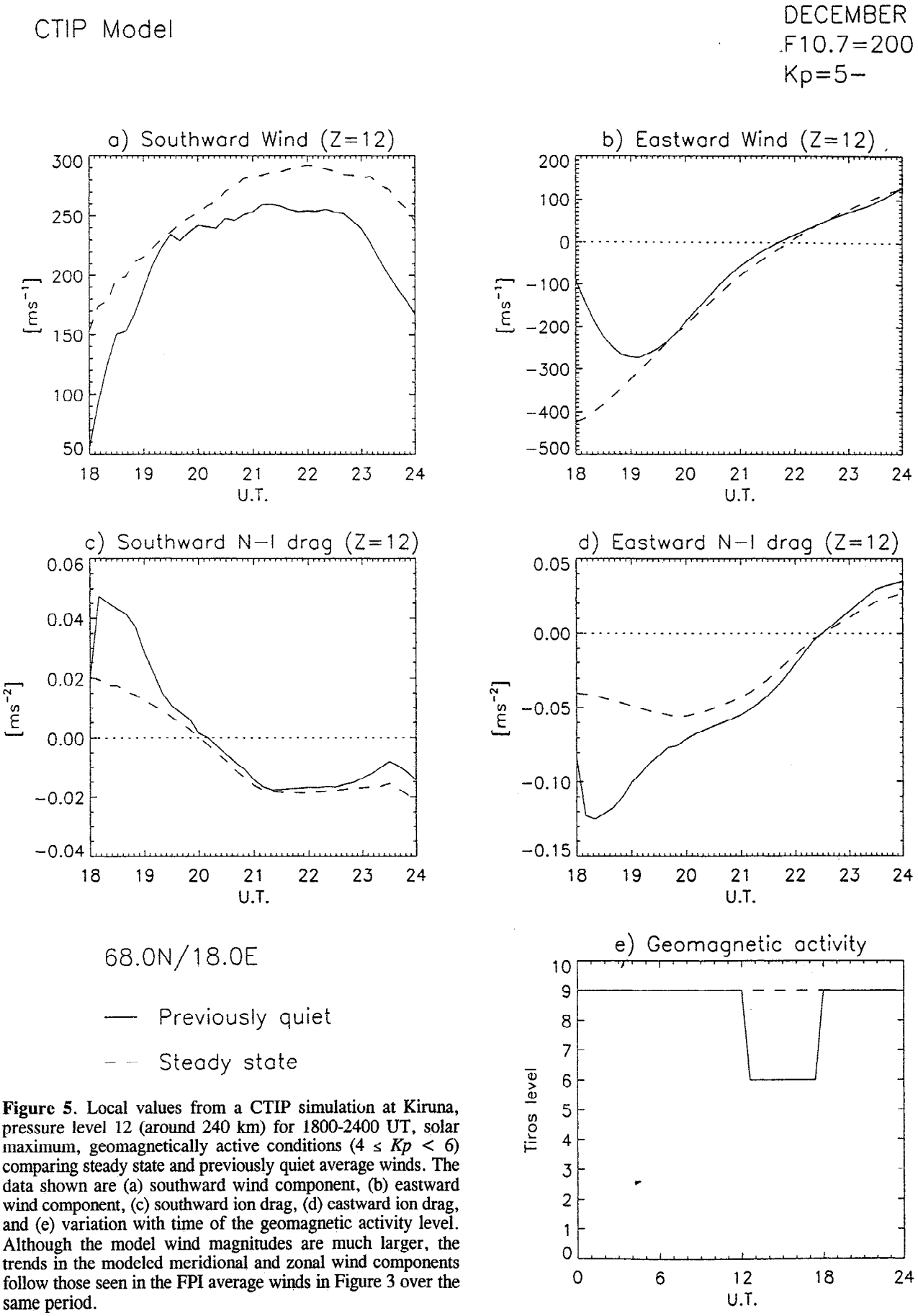

Figure 5. Local values from a CTIP simulation at Kiruna, pressure level 12 (around 240 km) for 1800-2400 UT, solar maximum, geomagnetically active conditions ($4 \leq Kp < 6$) comparing steady state and previously quiet average winds. The data shown are (a) southward wind component, (b) eastward wind component, (c) southward ion drag, (d) eastward ion drag, and (e) variation with time of the geomagnetic activity level. Although the model wind magnitudes are much larger, the trends in the modeled meridional and zonal wind components follow those seen in the FPI average winds in Figure 3 over the same period.

dominant term. It should be noted that the expression for Joule heating applies to an electric field in a stationary medium. However, here the medium is moving with velocity $\mathbf{U}_n$ which means that the expression should be used in the neutral wind frame and not in the Earth frame. In other words, the true Joule heating rate is **J.E'** and not **J.E**. The equation for the true Joule heating rate is derived by expanding **J.E'** using a current density, **J**, that is given by

$$\mathbf{J} = \sigma_p \mathbf{E}' + \sigma_h \mathbf{b}\hat{}\mathbf{E}'. \quad (2)$$

Here **b** is the unit vector in the direction of the magnetic field, and any electric field component parallel to **b** is assumed to be negligible while σ_p and σ_h are the Pedersen and Hall conductivities, respectively. Equation (3) gives the expansion of the Joule heating term, **J.E'**. In accordance with *Thayer et al.* [1995] the integral is given in terms of **E** since this is the measurable electric field in the Earth frame. The term $\sigma_p \mathbf{E}^2$ is used to calculate the Joule heating when it is assumed that the neutral wind is zero. However, if the neutral wind is not zero, then the term $\sigma_p \mathbf{E}.(\mathbf{U}_n\hat{}\mathbf{B})$ which has been called the Pedersen term, has been shown by *Thayer et al.* [1995] to be potentially large enough to reduce significantly the net flux into the ionosphere.

$$\int \mathbf{J}.\mathbf{E}'\, dz = \int [\sigma_p \mathbf{E}^2 + 2\sigma_p \mathbf{E}.(\mathbf{U}_n\hat{}\,\mathbf{B}) + \sigma_p(\mathbf{U}_n\hat{}\,\mathbf{B})^2]\, dz. \quad (3)$$

The second term of equation (1) represents the rate of change of kinetic energy of the neutral gas through collisions with the ions, in other words, the mechanical energy transfer rate. This term is expanded and given as equation (4). The term $\sigma_h |\mathbf{B}|(\mathbf{U}_n.\mathbf{E})$, called the Hall term, has been shown to be an order of magnitude smaller than the Pedersen term [*Thayer et al.*, 1995].

$$-\int \mathbf{J}.(\mathbf{U}_n\hat{}\,\mathbf{B})\, dz = -\int [\sigma_p \mathbf{E}.(\mathbf{U}_n\hat{}\,\mathbf{B}) + \sigma_p(\mathbf{U}_n\hat{}\,\mathbf{B})^2 - \sigma_h |\mathbf{B}|(\mathbf{U}_n.\mathbf{E})]\, dz. \quad (4)$$

An illustration of the relative importance of the Joule heating and mechanical energy transfer rate at high latitudes, and thus also the significant contribution of the neutral wind, is given in Figures 6a and 6b. The figures show a slice from dusk to dawn (1800-0600 LT meridian)for latitudes above 60°N, using the same layout as Figure 3 from *Thayer et al.* [1995] which shows the three energy terms of equation (1) in height-integrated form. Figure 6a shows the CTIP simulations for the ss(q) at 1800 UT, while Figure 6b shows the pa(q) simulation. This time has been chosen because it is just after the geomagnetic activity level has been reduced to the steady state level for the pa(q) simulation. The Thayer et al. simulation uses a cross cap potential difference of 60 kV, representing quiet to moderate conditions, while the CTIP steady state simulation uses 26 kV to represent $Kp = 1+$. The maximum value of all the energy terms in Figures 6a and 6b is 3 mW/m^2, which is consistent with *Thayer et al.*[1995].

As might be expected, the magnitudes of all three terms are larger for the pa(q) simulation (Figure 6b). In both cases the magnitudes of all of the energy terms are larger on the duskside than on the dawnside. Also, the net **J.E** term is positive over the whole polar region, that is, the ionosphere is a net sink of energy, except for a small region of the polar cap on the dawnside. The peak Joule heating rate, located at around 74°N on the duskside, is 25% larger for the pa(q) case as for the ss(q) case. This is entirely due to a difference in σ_p and $\mathbf{U}_n$ because **E** is the same for both simulations. The difference in the values of **J.E** shown in Figures 6a and 6b indicates how important the previous conditions are for determining the instantaneous load that the ionosphere presents to the magnetosphere.

The noticeably large dawn-dusk asymmetry in the energy terms can be attributed to the Coriolis force which favors a clockwise vortex [*Fuller-Rowell and Rees*, 1984]. Thus a neutral gas parcel is kept within the dusk cell and can therefore pick up a great deal of momentum from the plasma. In contrast, a gas parcel in the dawn cell, which is an anticlockwise vortex, tends to be diverted outward by the Coriolis force and therefore picks up much less momentum. Comparison of Figures 6a and 6b shows that within the polar cap, that is, over the range of latitudes 85°-90°N on the dawnside, the **J.E** term for the pa(q) case can in some places be up to 75% larger than the ss(q) case, and in others be negative. This is largely because, unlike the Joule heating term, the mechanical energy term can be negative (i.e., energy transformation from kinetic to electromagnetic) and is a highly significant component of the **J.E** term for the pa(q) case. Especially over the polar cap region, the magnitude of the Joule heating term is similar to the mechanical energy term.

Furthermore, Figure 6c shows a comparison between the apparent Joule heating, $\sigma_p \mathbf{E}^2$ (which is the commonly used simplification that uses the electric field in the Earth frame and assumes a zero neutral wind), and the real Joule heating, $\sigma_p \mathbf{E}'^2$, which illustrates clearly the problem if the neutral wind is ignored in empirical measurements of energy flux. This is even more strikingly illustrated by Plate 4 from *Thayer et al.* [1995].

In order to monitor how the energy terms vary with time, Figure 7 shows the same dusk to dawn slice (1800-0600 UT) at 2100 UT, 3 hours after the geomagnetic activity has been reduced for the pa(q) simulation. Figure 7a shows that there is little change in the Joule heating rate compared with Figure 6a, which is to be expected, because this is the steady state condition. Any change will be due to the rotation of the Earth, and thus the location of the ionospheric convection pattern which is centered on the geomagnetic pole. For example, the location of the peak Joule heating rate has moved from 74°N in the dusk sector at 1800 UT to around 67°N at 2100 UT. In contrast, comparison of Figures 6b and 7b shows that all the terms for the pa(q) simulation are getting smaller as the atmosphere recovers to the quiet situation.

An important point about Figures 6a and 6b is that the solar heating flux, electric field, and particle precipitation patterns for both cases are exactly the same. Thus if there is no knowledge of the geomagnetic history and its effect on the neutral atmosphere, or it is ignored, then instantaneous measurements of the energy budget might be interpreted as showing an anomaly between the two cases. This is not a hypothetical problem because a significant number of radar studies in the past have assumed that the neutral wind is zero owing to the lack of neutral wind measurements over the appropriate height region and used $\sigma_p \mathbf{E}^2$ to calculate the Joule heating rate [e.g., *Foster et al.*, 1983; *Kamide and Kroehl*, 1987; *Fontaine and Peymirat*, 1996]. In such a case it is quite possible that an unnecessary mechanism might be suggested to explain the difference. For example, the **J.E** term and Joule heating term are almost equal for the ss(q) case (Figure 6a), so the changes in ion and neutral temperatures associated with

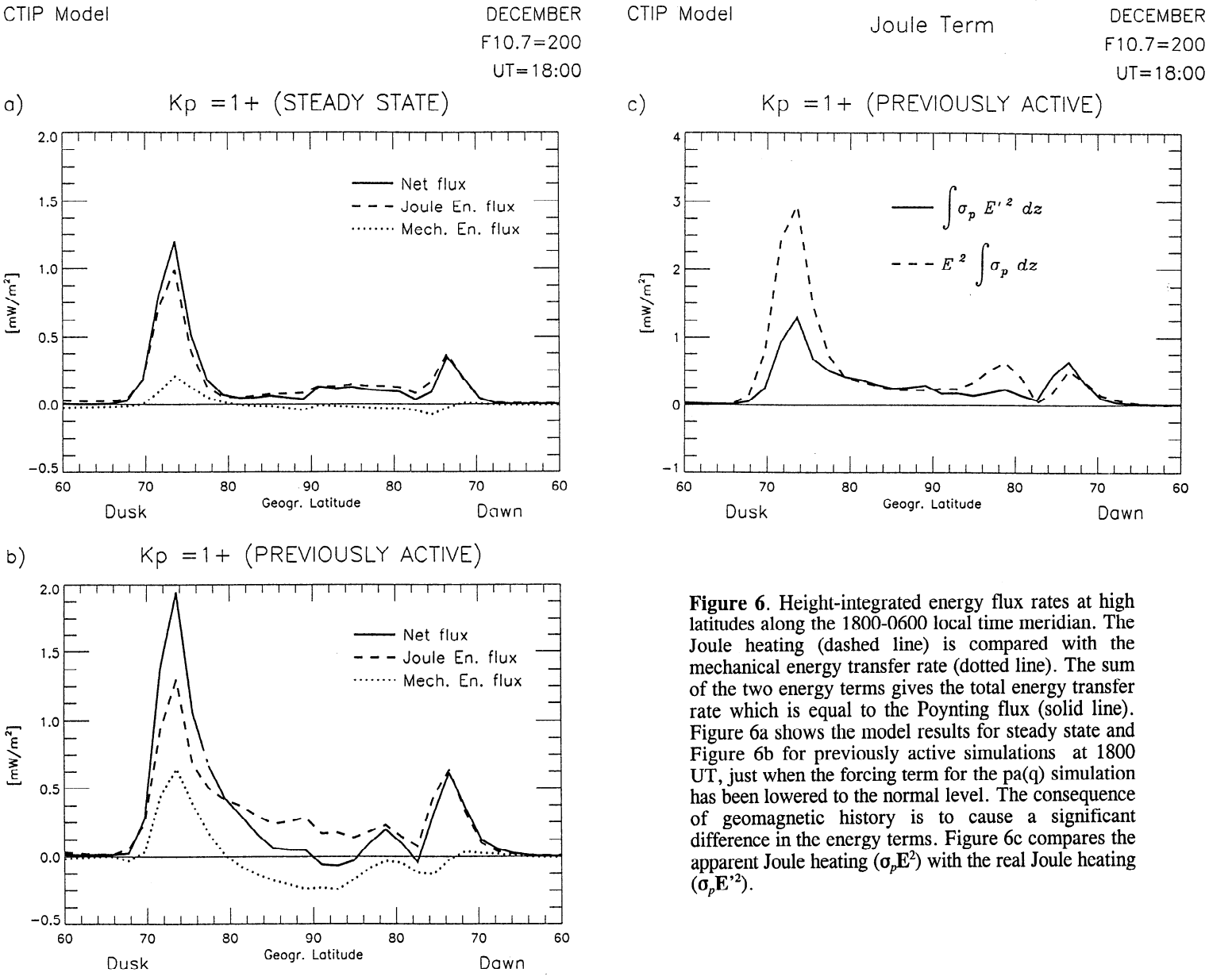

Figure 6. Height-integrated energy flux rates at high latitudes along the 1800-0600 local time meridian. The Joule heating (dashed line) is compared with the mechanical energy transfer rate (dotted line). The sum of the two energy terms gives the total energy transfer rate which is equal to the Poynting flux (solid line). Figure 6a shows the model results for steady state and Figure 6b for previously active simulations at 1800 UT, just when the forcing term for the pa(q) simulation has been lowered to the normal level. The consequence of geomagnetic history is to cause a significant difference in the energy terms. Figure 6c compares the apparent Joule heating ($\sigma_p E^2$) with the real Joule heating ($\sigma_p E'^2$).

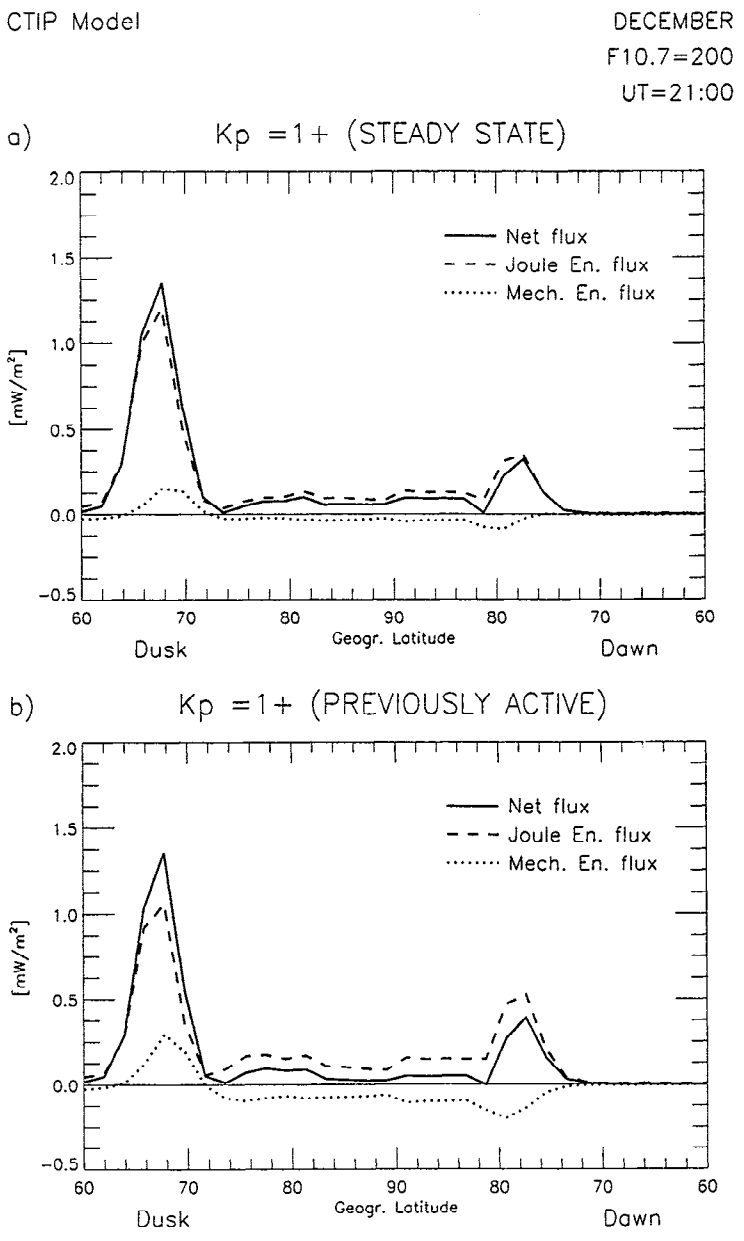

Figure 7. Same layout as for Figures 6a and 6b, showing the model results for (a) steady state and (b) previously active simulations at 2100 UT, 3 hours after the forcing term has been lowered to the normal level. The pa(q) simulation has recovered to be almost the same as the ss(q) simulation.

Joule heating will be compatible with the measurements of **J** and **E**. However, for the pa(q) case, **J.E**≠**J.E'**; thus it will be noticed that the ionosphere is drawing a great deal more energy from the magnetosphere than is being dissipated in Joule heating.

Similarly to Figures 6 and 7, Figure 8 shows a slice from dusk to dawn for latitudes above 60°N from the CTIP simulations of active conditions at 1800 UT, comparing the pq(a) with the ss(a) case, while Figure 9 shows the results 3 hours later, at 2100 UT. The energy terms for the pq(a) simulation at 1800 UT (Figure 8b) are significantly smaller than for the ss(a) (Figure 8a) despite having the same solar heating flux, electric field, and particle precipitation patterns. Again, this is not surprising when the geomagnetic history is considered. The main sinks of magnetospheric energy are in the dawn and dusk sectors where the maximum value of **J.E** occurs for the ss(a) case at nearly 30 mW/m^2 on the duskside at 68°N. This is an order of magnitude larger than the quiet to moderate simulation of *Thayer et al.* [1995]. However, in the polar cap region the energy fluxes are relatively very small. Thus it should be noted that an estimate of the average energy flux over the whole polar region works out to be around 100 GW, which is comparable with a power input of 78.4GW quoted by *Evans et al.* [1987] for the precipitation pattern with an average Kp=5- that is used by CTIP.

On the duskside the **J.E** term has two peaks at about 68°N and 75°N for both simulations. The peaks are at a lower latitude than for the quiet simulations of Figures 6 and 7 owing

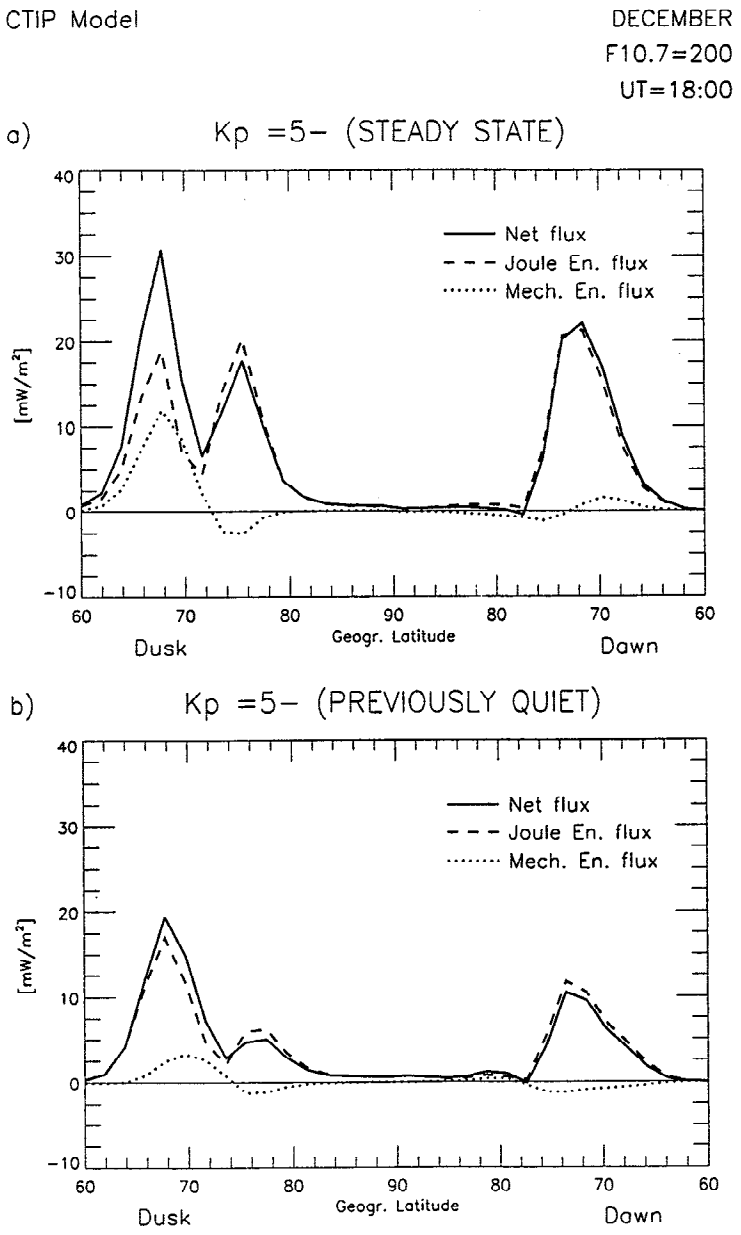

Figure 8. Same layout as for Figures 6a and 6b showing the model results for (a) steady state and (b) previously quiet simulations at 1800 UT, just when the forcing term for the pq(a) simulation has been raised to the normal level.

to the expansion of the auroral oval with increasing geomagnetic activity. After 3 hours the two simulations are similar, as can be seen in Figure 9. It is worth pointing out that there may not be any simple rule for which geomagnetic history conditions it is reasonable to assume a zero neutral wind when calculating the energy terms. The assumption of a zero neutral wind for the pq(a) case (Figure 8b) will not make a significant difference in calculating the Joule heating because the **J.E** term is almost equal to the Joule heating term. However, for the ss(a) case the ionospheric load on the magnetosphere is not dissipated solely by Joule heating. This is in contrast with the quiet simulations shown in Figures 6a and 6b, where assuming a zero neutral wind will not be significant for the ss(q) case but will be important for the pa(q) case.

5. How Far Back in Time Must the Geomagnetic History be Considered?

Comparison of Figures 7a and 7b and also Figures 9a and 9b indicates that the perturbed model atmosphere takes just over 3 hours to recover to the steady state condition. Returning to the real world, Figure 10 shows a comparison of average winds where the previous 3, 6, or 12 hours have been used to provide a geomagnetic history. The data shown are for active conditions ($4 \leq Kp < 6$) at solar maximum where the previous 3/6 or 12 hours were, on average, quieter, that is, $Kp < 4$. Generally there is little difference between these average winds; indeed, the 12 hour geomagnetic history average is almost identical with the 6 hour geomagnetic history average and therefore

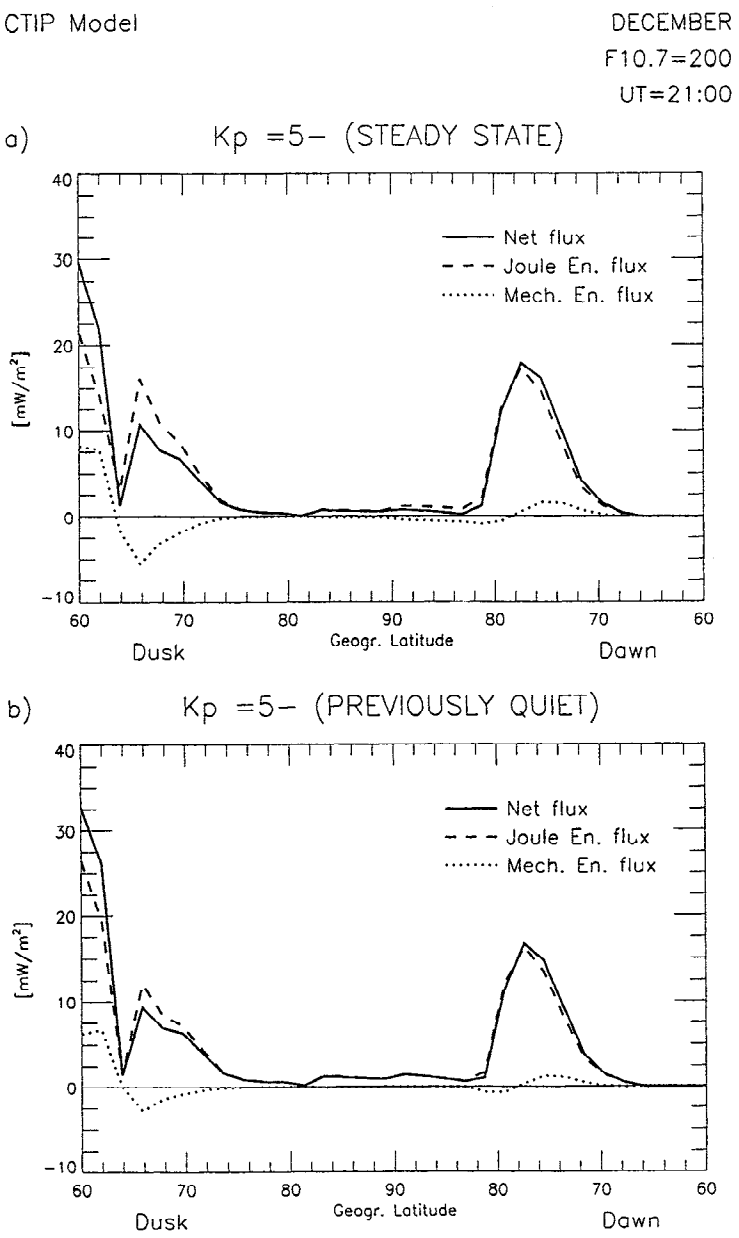

Figure 9. Same layout as for Figure 6a and 6b showing the model results for (a) steady state and (b) previously quiet simulations, at 2100 UT, 3 hours after the forcing term has been raised to the normal level. The pq(a) simulation has recovered to be almost the same as the ss(q) simulation.

indicates that 12 hours is an unnecessarily long period to be considered. This implies that it is mainly the previous 3 hours that are the most important, which agrees with the model simulation results.

It can be seen from comparing different 3 hour periods of FPI average wind data that the influence of geomagnetic history is strongly dependent on the local time, and therefore location. For example, the zonal winds in the period between 1800 and 0000 UT are hardly changed by looking back further than 3 hours previously, whatever the level of geomagnetic activity or whether the previous activity levels were higher or lower. However, there is a distinct, statistically significant difference in the zonal winds between 1400 and 1800 UT. This can be attributed to the spatial distribution of electron density because the electron density is proportional to the neutral-ion collision frequency, and therefore determines the speed with which the neutrals respond to ionospheric forcing [*Rishbeth and Garriott*, 1969]. Subsequently, the speed with which the previously active or quiet thermosphere returns to a steady state condition will also be affected. Using this argument, it is expected that there will be a dependency on solar activity and season as well.

6. Conclusions

Previous investigators have shown that the response of plasma flows to changes in the high-latitude electric field is almost immediate. In other words, the plasma velocity has no

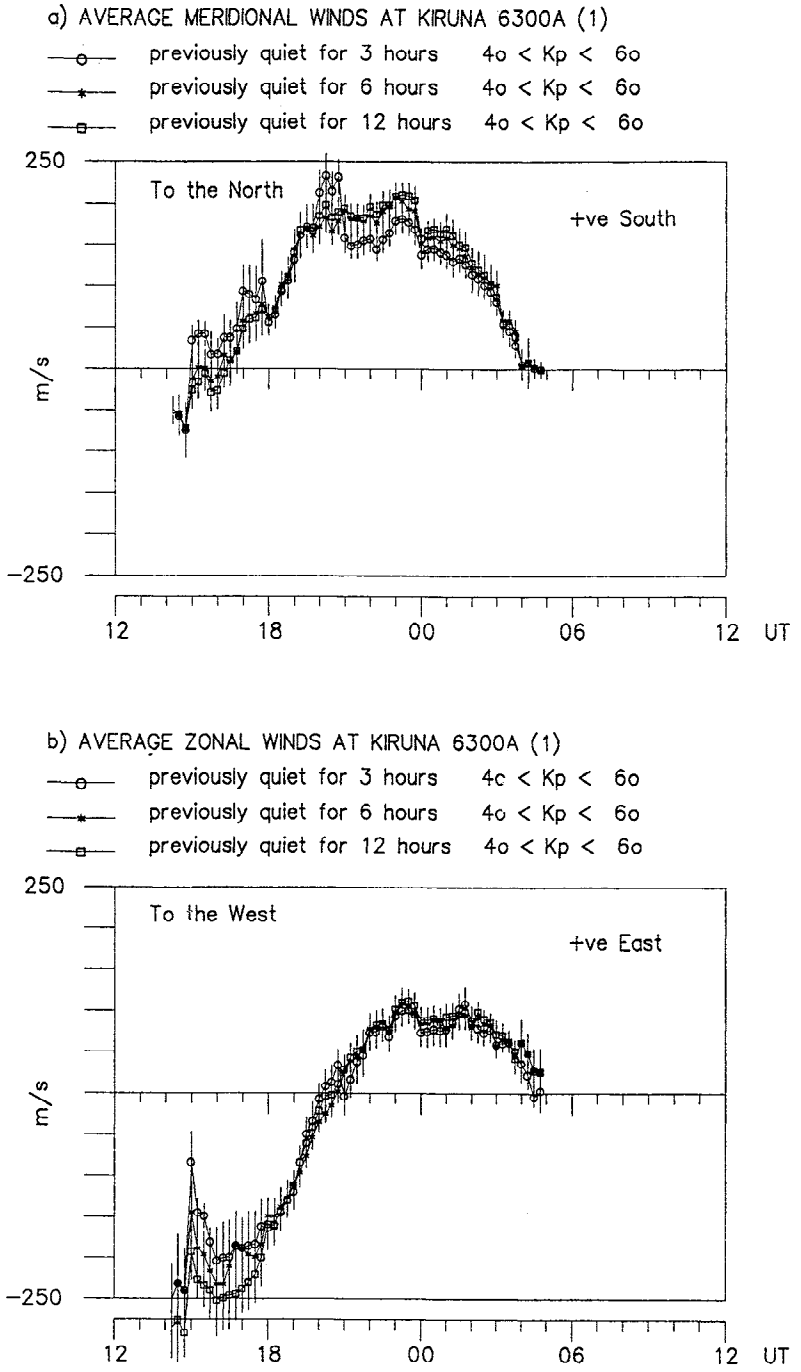

Figure 10. A comparison of average winds where the previous 3, 6, or 12 hours have been used to provide a geomagnetic history. Generally there is little difference between these average winds, which implies that it is mainly the previous 3-6 hours that are the most important.

significant geomagnetic history. In contrast, the neutral gas has a long memory for what has occurred before. The consequence of this has been shown using average winds calculated from a large database of neutral winds measured using a FPI at Kiruna, Sweden, and also model simulations using the CTIP model. The results may be summarized by the following three points:

1. A previously active condition will not have the same neutral winds, temperature, composition, energy, and momentum levels as a steady state, or a previously quiet condition, despite having the same current magnetospheric forcing. These variables will be more typical of a level of forcing intermediate to the previous and current level for several hours after the change in forcing. Therefore the geomagnetic history must be taken into consideration in interpreting the behavior of the upper atmosphere. When modeling or using empirical model data, this can be done by giving enough lead time to allow for previous activity.

2. In general, the previous 3-6 hours provide the most important influence on the thermosphere and energy dissipation rates, though it is expected that the local time and the location of the site will affect the strength of the geomagnetic history effects and the time taken to revert to steady state conditions.

3. The model results show that momentum transfer and Joule heating can be severely overestimated/- underestimated if steady state conditions are assumed when actually the previous activity levels were higher/lower. In particular, the common practice of setting the neutral wind to zero to simplify calculations means that both the inertia and the dynamo action of the neutral wind are overlooked. (In other words, the neglect of the neutral wind presumes that the steady state case is the same as the previously active or quiet cases.) In such a case the load that the ionosphere presents to the magnetospheric dynamo will be calculated incorrectly. As a result, other mechanisms may be invoked unnecessarily.

Acknowledgments. The authors would like to thank the FPI team at the Atmospheric Physics Laboratory for building and maintaining the instruments that provide this valuable long-term database of thermospheric wind measurements. The instruments and the CTIP model are funded by the Particle Physics and Astronomy Research Council. The assistance of the Institutet för Rymdfysik at Kiruna, where the instrument is located, is gratefully acknowledged. The *Kp* indices used in the analysis come from the World Data Centre. The authors also acknowledge the very helpful comments of the referees.

Michel Blanc thanks Arthur D. Richmond and Christophe Peymirat for their assistance in evaluating this paper.

References

Aruliah A.L., A.D. Farmer, D. Rees, andU. Brändström, The seasonal behaviour of high-latitude thermospheric winds and ion velocities observed over one solar cycle, *J. Geophys. Res.*, *101*, 15,701-15,711, 1996.

Brekke, A., Electric fields, Joule and particle heating in the high latitude thermosphere, *J. Atmos. Terr. Phys.*, *38*, 887-895, 1976.

Deng, W., T.L. Killeen, A.G. Burns, R.G. Roble, J.A. Slavin, and L.E. Wharton, The effects of neutral inertia on ionospheric currents in the high-latitude thermosphere following a geomagnetic storm, *J. Geophys. Res.*, *98*, 7,775-7,790, 1993.

Etemadi, A., S.W.H. Cowley, M. Lockwood, B.J.I. Bromage, D.M. Willis, and H. Luhr, The dependence of high-latitude dayside ionospheric flows on the north south component of the IMF- A high time resolution correlation-analysis using EISCAT, POLAR and AMPTE UKS and IRM data, *Planet. Space Sci.*, *36*, 471-498, 1988

Evans, D.S., T.J.fuller-Rowell, S.Maeda, J.Foster, Specification of the heat input to the thermosphere from magnetospheric processes using TIROS/NOAA auroral particle observations, *Advances in the Astronautical Sciences*, *65*, 1649-1667, 1987.

Field, P.R., H. Rishbeth., R. Moffett., D.W. Idenden, T.J. Fuller-Rowell, G.H. Millward, and A.D. Aylward, Modelling composition changes in *F*-layer storms, *J. Atmos. Sol. Terr. Phys.*, *60*, 523-543, 1998.

Fontaine, D., and C. Peymirat, Large-scale distributions of ionospheric horizontal and field-aligned currents inferred from EISCAT, *Annales Geophys.*, *14*, 1,284-1,296, 1996.

Foster, J.C., J.-P. St.-Maurice, and V.J. Abreu, Joule heating at high latitudes, *J. Geophys. Res.*, *88*, 4,885-4,896, 1983.

Foster J.C., J.M. Holt, R.G. Musgrove, and D.S. Evans, Ionospheric convection associated with discrete levels of particle precipitation, *Geophys.Res.Lett.*, *13*, 656-659, 1986.

Fuller-Rowell, T.J., and D.S.Evans, Height integrated Pedersen and Hall conductivity patterns inferred from the TIROS-NOAA satellite data, *J. Geophys. Res.*, *92*, 7,606-7,618, 1987.

Fuller-Rowell, T.J., and D. Rees, Interpretation of an anticipated long-lived vortex in the lower thermosphere following simulation of an isolated substorm, *Planet. Space Sci.*, *32*, 69-85, 1984.

Fuller-Rowell, T.J., D. Rees, S. Quegan, R.J. Moffett, and G.J. Bailey, Interactions between neutral thermospheric composition and the polar ionosphere using a coupled ionosphere-thermosphere model, *J. Geophys. Res.*, *92*, 7,744-7,748, 1987.

Fuller-Rowell, T.J., D. Rees, S. Quegan, R.J. Moffett, M.V. Codrescu, and G.H. Millward, A coupled thermosphere-ionosphere model (CTIM), *Aeronomical Models of the Ionosphere, STEP Handbook*, edited by R.W. Schunk, 217-238,Utah State University, Logan, Utah, 1996.

Gary, J.B., R.A. Heelis, W.B. Hanson, and J.A. Slavin, Field-aligned Poynting flux observations in the high-latitude ionosphere, *J. Geophys. Res.*, *99*, 11,417-11,427, 1994.

Kamide, Y., and H.W. Kroehl, A concise review of the utility of ground-based magnetic recordings for estimating the Joule heat production rate, *Ann. Geophys.*, *5A*, 535-542, 1987.

Kelley, M.C., D.J. Knudsen, and J.F. Vickrey, Poynting flux measurements on a satellite: A diagnostic tool for space research, *J. Geophys. Res.*, *96*, 201-207, 1991.

Lu, G., A.D. Richmond, B.A. Emery, and R.G. Roble, Magnetosphere-ionosphere-thermosphere coupling: Effect of neutral winds on energy transfer and field-aligned current, *J. Geophys. Res.*, *100*, 19643-19659, 1995.

Lyons, L.R., T.L. Killeen, and R.L. Walterscheid, The neutral wind "flywheel" as a source of quiet-time, polar cap currents, *Geophys. Res. Lett*, *12*, 101-104, 1985.

Millward, G.H., R.J. Moffett, S. Quegan, and T.J. Fuller-Rowell, A coupled thermosphere-ionosphere-plasmasphere model (CTIP), in *Aeronomical Models of the Ionosphere, STEP Handbook*, edited by R.W. Schunk, 239-280,Utah State University, Logan, Utah, 1996.

Müller-Wodarg I., and A.D.Aylward, The influence of tides on composition of the thermosphere, *Adv. Space Res.*, *21*, 807-810, 1998.

Rishbeth H., and O.K.Garriott, Introduction to Ionospheric Physics, *Academic*, San Diego, Calif.,1969.

Rishbeth H., The ionospheric *E*-layer and *F*-layer dynamos- A tutorial review, *J. Atmos. Sol. Terr. Phys.*, *59*, 1,873-1,880, 1997.

Rishbeth and Müller-Wodarg, Vertical circulation and thermospheric composition: A modelling study, *Ann. Geophys.*, *17*, 794-805, 1999.

Thayer, J.P., J.F. Vickrey, R.A. Heelis, J.B. Gary, Interpretation and modelling of the high-latitude electromagnetic energy flux, *J. Geophys. Res.*, *100*, 19,715-19,728, 1995.

A. L. Aruliah and I. C. F. Müller-Wodarg, Atmospheric Physics Laboratory, University College London, 67-73, Riding House Street, London W1P 7PP, England. (anasuya@apg.ph.ucl.ac.uk, ingo@apg.ph.ucl.ac.uk)

J. Schoendorf, Mission Research Corporation, 1, Tara Boulevard, Nashua, NH 03062. (jschoendorf@mrcnh.com)

(Received September 4, 1998; revised July 5, 1999; accepted July 10, 1999.)